CHAPTER 4

RESULTS AND DISCUSSIONS

4.1 Characterization

4.1.1 TEM

The following images, Figures 4.1 to 4.4 reflect the bulk (TEM) images of Pt/C, Pt/Nb_2O_5-C, Pt/Ta_2O_5-C and Pt/ZrO_2-C at low magnification (28500X) while Figures 4.5 to 4.8 were taken at high magnification (73000X). A bar at the bottom right of the each low magnification images represents 0.5µm and 1.0µm at the high magnification. The grey area resembles the dispersion of Vulcan carbon XC-72, dark tiny spots are Pt particles and dark larger crystals are metal oxides. However, it is hard to distinguish between the metal oxides and Pt particles on the TEM image. Figure 4.1 reveals how the preparation method used to prepare the catalyst was unable to completely reduce $PtCl_6^{2-}$ to metallic platinum. This can be seen by the numerous darkest spots which have agglomerated forming large crystals instead of tiny dark spots.

The darkest spots represent the Pt particles and the grey portion resembles the Vulcan carbon XC-72 support. The micrograph at a magnification of 28500X depicts a slightly homogenous material, however, it also reflects the presence of platinum crystals surrounding the carbon (shown in Figure 4.1). Figure 4.2 depicts weak platinum-metal oxides interactions. The Pt particles are agglomerated and the niobium pentoxide is not well dispersed on the Vulcan carbon XC-72 support. The agglomerated Pt crystals are of uneven size. The slightly darker regions (not the greyish region) on the Figure 4.3 micrograph resemble the coverage of Ta_2O_5 on carbon and the tiny dark spots are the Pt particles. Although within this darker region it is much more complex to distinguish between Pt and Ta_2O_5. The grey is the Vulcan carbon XC-72 support.

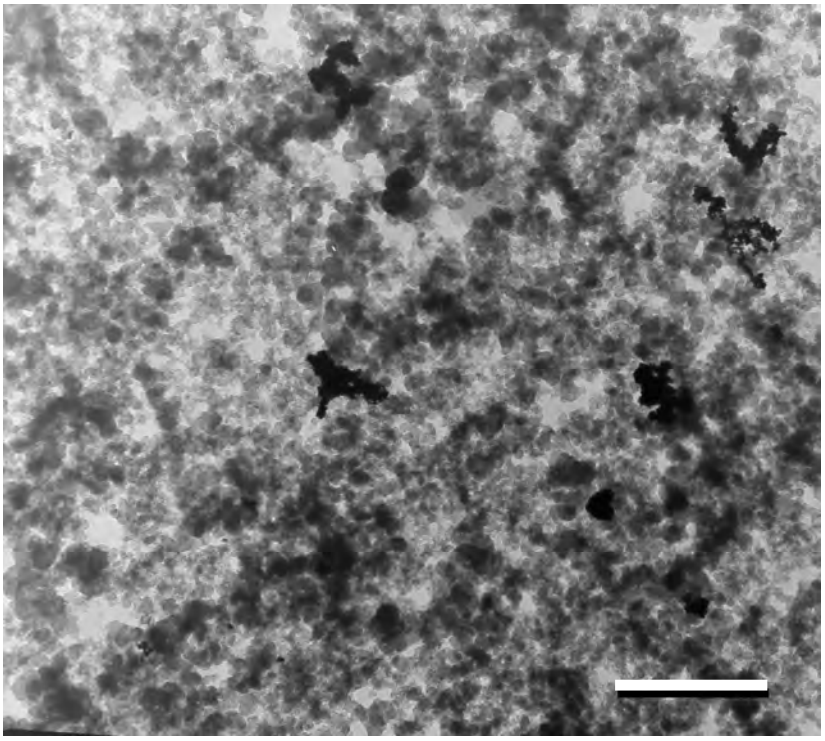

Figure 4.1 TEM image of Pt/C under 28500X magnification

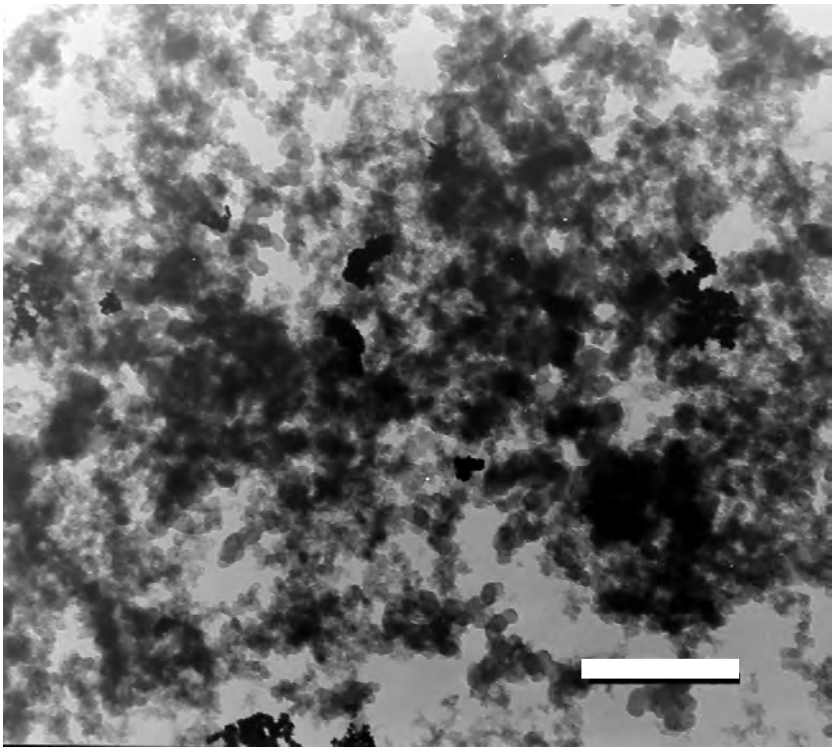

Figure 4.2 TEM Image of Pt/Nb_2O_5-C under 28500X magnification

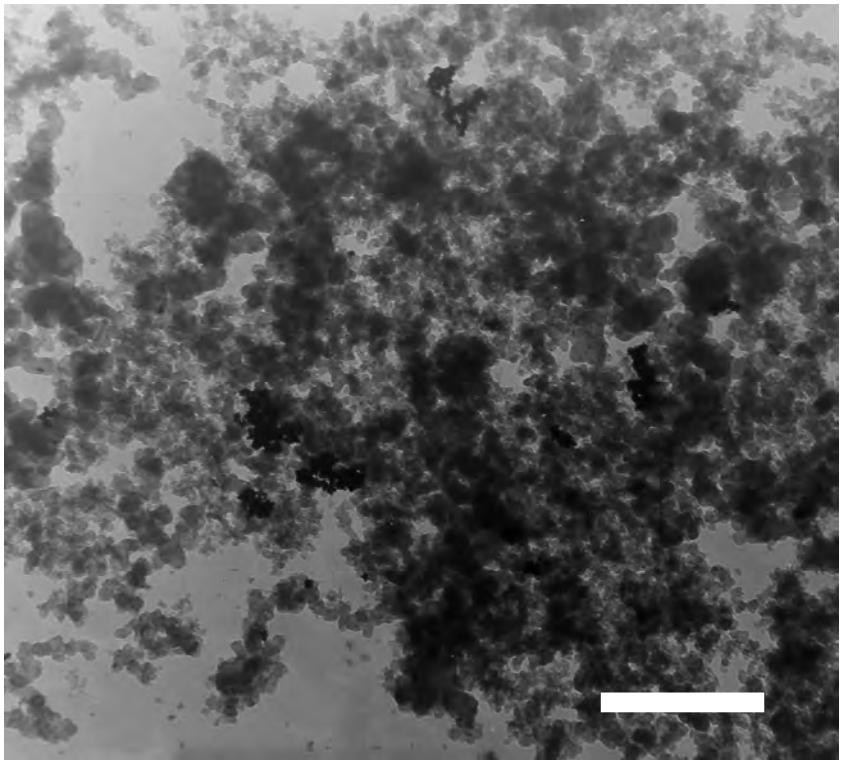

Figure 4.3 TEM Image of Pt/Ta_2O_5-C under 28500X magnification

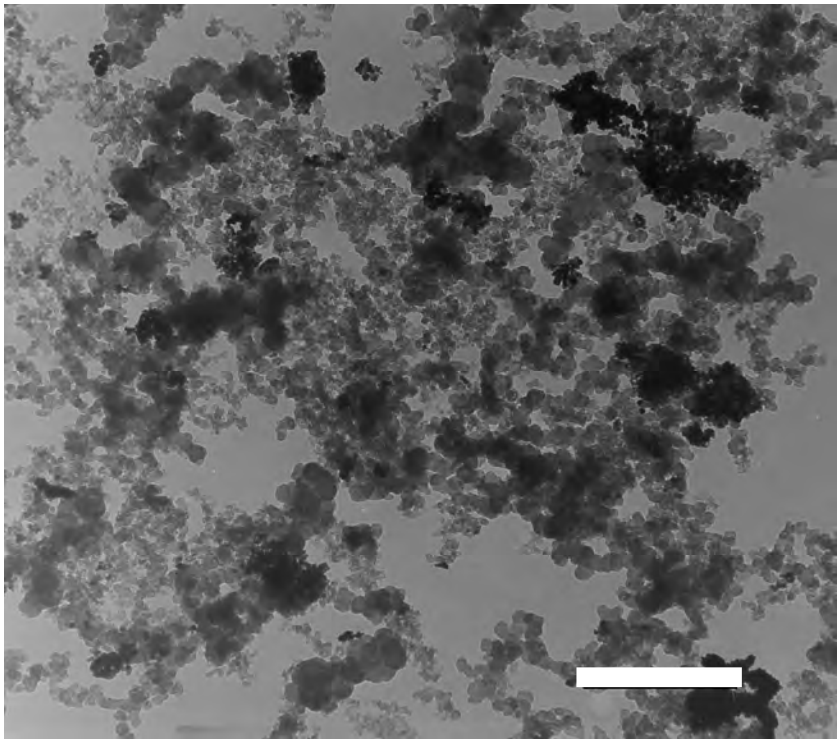

Figure 4.4 TEM Image of Pt/ZrO_2-C under 28500X magnification

The sparse distribution of catalyst material for Pt/ZrO_2-C in Figure 4.4 may be due to the preparation of the catalyst material and preparation of the sample for transmission electron microscopy. When we tried out the exact catalyst preparation method without any alterations as communicated by Chen et al. [129] this resulted in the transmission electron micrographs in Figures 4.5 - 4.8, whereas when we made a few adjustments as communicated in 3.2.1, this resulted in the micrographs shown in Figures 4.1 to 4.4.

Though the platinum is found all over the carbon support, it is also noted that the platinum particles vary in size.The original form of the metal oxides played a great role in their TEM images thus the Pt/ZrO_2-C material was less likely to agglomerate since ZrO_2 nanopowder have a particle size of less than 100nm when compared to the particle size of less than 5µm for Nb_2O_5 and Ta_2O_5. Pt/Nb_2O_5-C and Pt/Ta_2O_5-C revealed a lot of agglomerates while no uniform distribution of Pt particles was experienced on Pt/ZrO_2-C.

In this image, Figure 4.6, the platinum is not well dispersed on the carbon because the carbon at the top right of the image is not exposed to any Pt crystals. Niobium pentoxides are agglomerated hence it is complex to precisely determine where platinum is more likely to be attached to the carbon or the niobium pentoxides. These large agglomerates of the niobium pentoxides will have a great effect on the surface area.

In Figure 4.7, the platinum is well dispersed on the carbon. However, tantalum pentoxides are agglomerated hence it is also observed that platinum is more attracted or more visible in the surrounding areas of tantalum pentoxides. Homogenous distributions of platinum and zirconium particles over the carbon support are observed. Uniform sizes of the zirconium dioxides are noted in Figure 4.8.

The presence of tantalum pentoxide and niobium pentoxide did not favour the good distribution of Pt particles on the carbon support, this was due to the minimal Pt-metal oxide interaction. Pt, Pt/Nb_2O_5 and Pt/Ta_2O_5 failed to disperse well over the entire available sites on the carbon. This limited and reduced the active sites (small EAS).

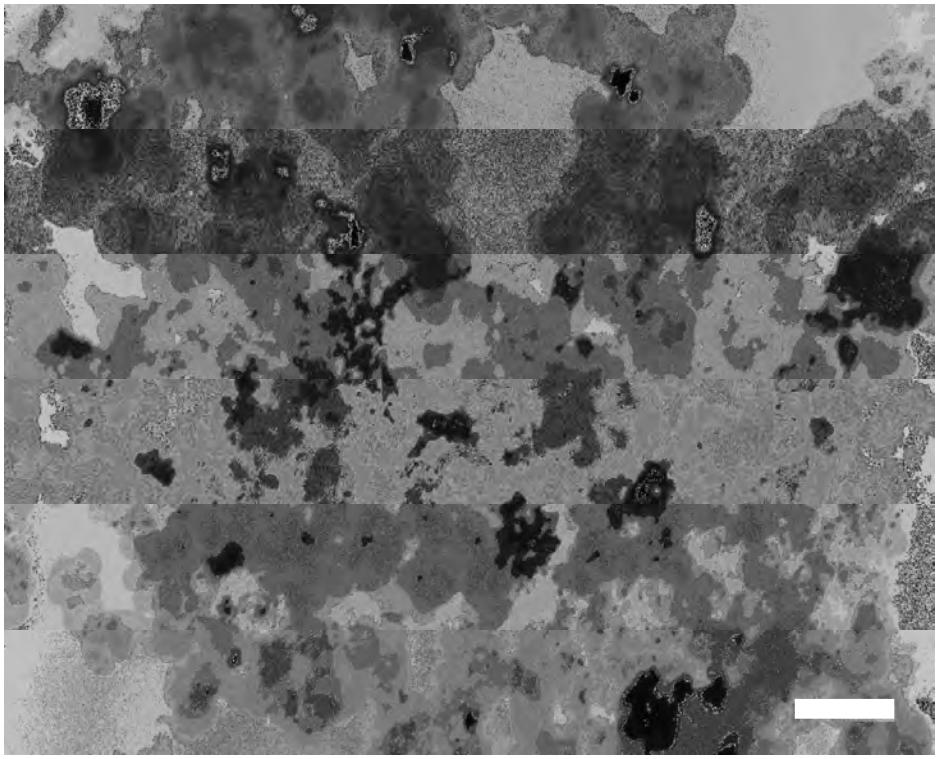

Figure 4.5 TEM Image of Pt/C under 73000X magnification

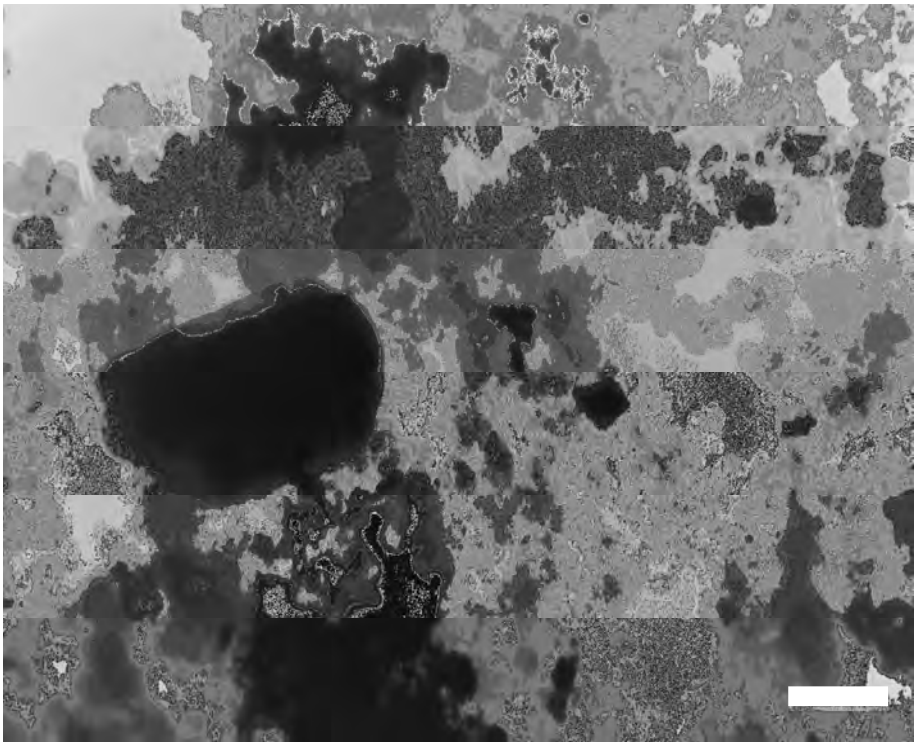

Figure 4.6 TEM Image of Pt/Nb_2O_5-C under 73000X magnification

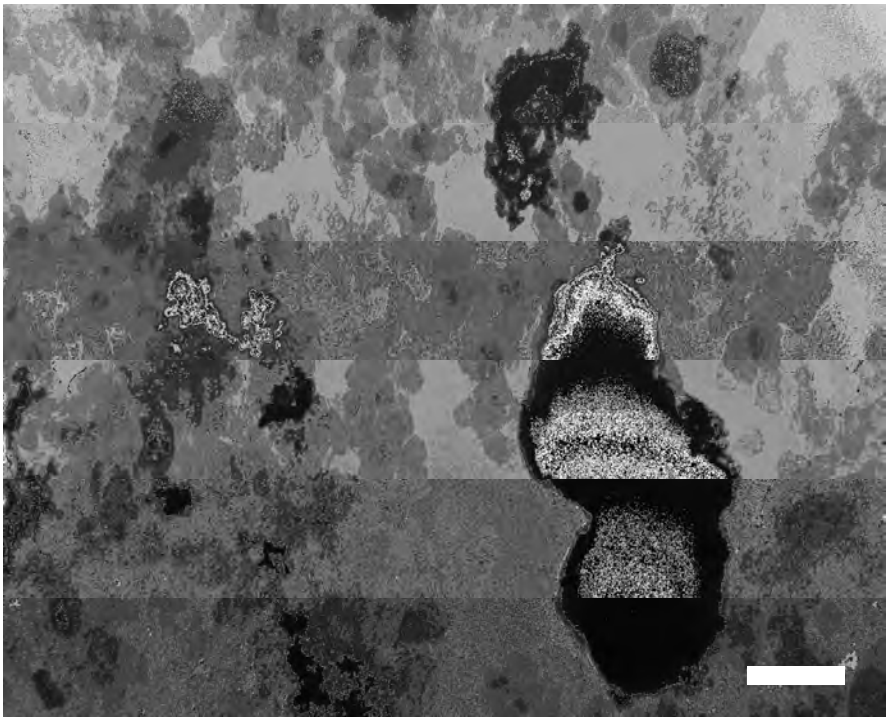

Figure 4.7 TEM Image of Pt/Ta_2O_5-C under 73000X magnification

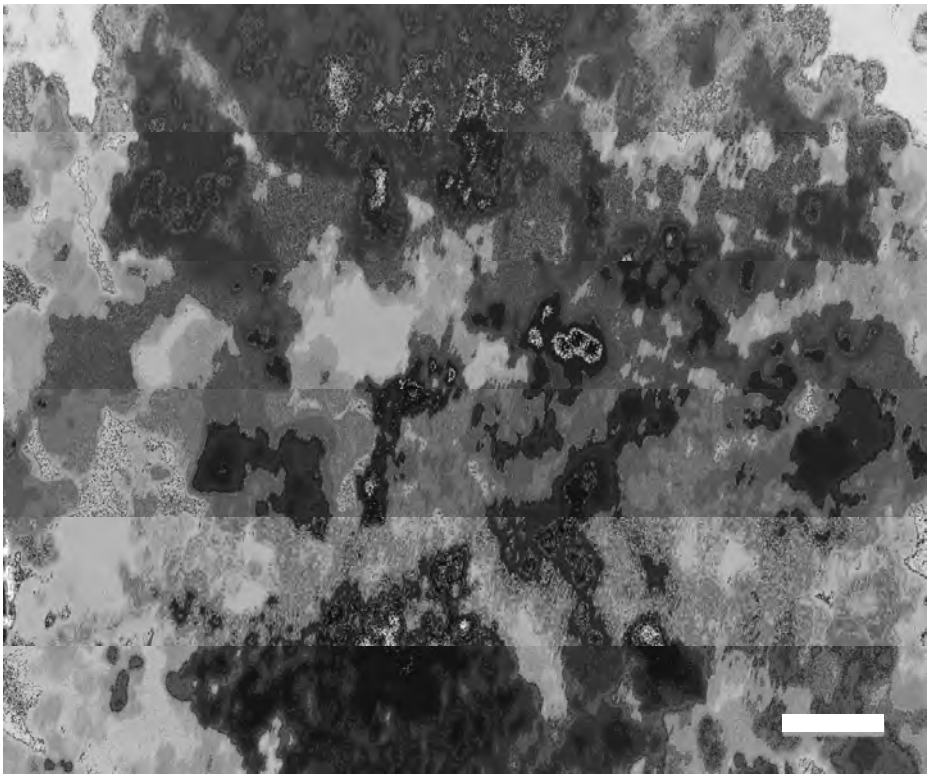

Figure 4.8 TEM Image of Pt/ZrO_2-C under 73000X magnification

In summary, observed from the TEM images it is seen that Pt particles appear more dispersed on carbon than on the metal oxides (Pt/Nb_2O_5-C, Pt/Ta_2O_5-C and Pt/ZrO_2-C). At low magnification it was difficult to distinguish between the different constituents of the catalyst materials in Pt/Nb_2O_5-C and Pt/Ta_2O_5-C, but TEM images of the fresh electrocatalysts are shown in Figures 4.1 to 4.4 where black spots corresponding to the magnification of 28500X were not clearly distinguishable from the carbon black support hence identification of different types of materials was complex.

The expected outcome was that there would be uniform sized platinum particles distributed uniformly on the catalyst support (M_xO_y), which was however not observed in all cases of this research. We observed that the metal (Zr, Ta, Nb) with higher atomic mass showed a much darker reflection on the TEM images, for example the Vulcan XC72 carbon had a greyish hue compared to tantalum pentoxide which had a much darker hue.

4.1.2 X-Ray Diffraction

Figure 4.9(a) reveals the XRD peaks for Vulcan XC72 carbon, and shows a peak at the 2theta position between 20 and 30˚ which is due to the carbon support.

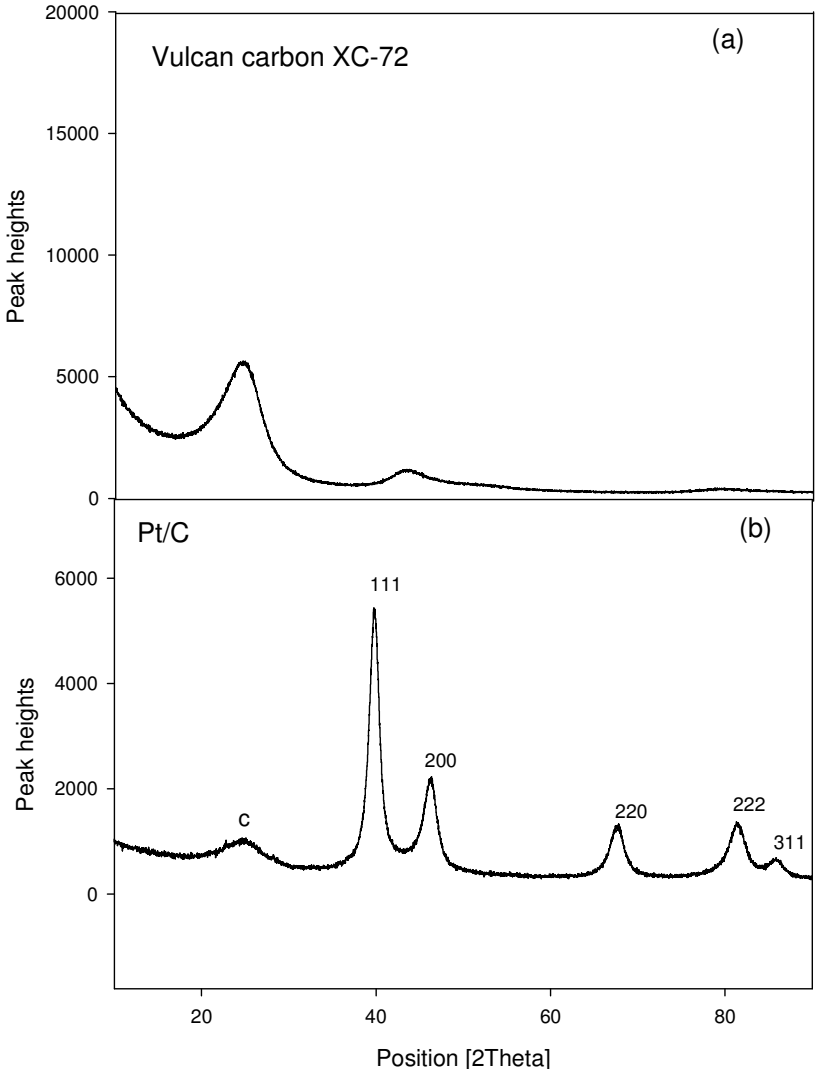

Figure 4.9 X-ray diffractographs of Vulcan carbon XC-72 (a) and Pt/C (b)

Figure 4.9(b) again shows carbon peak but it is diminished to a great extent due to platinum coverage of the carbon. The rest of the peaks on the Pt/C diffractograph are as a result of the Pt presence. The peaks corresponding to reflections at 2θ = 39.73° (111), 46.6° (200), 67.51° (220) 67.93° (222) and 81.3° (311) are indexed to the face-centered cubic structure of Pt crystallites. The Pt (111) plane contains hexagonally

packed Pt atoms and did not undergo surface reconstruction, unlike the Pt (100) and Pt (110) surfaces. However, the XRD peaks corresponding to Pt particles were superimposed on Vulcan carbon XC72 reflections at 2θ = 44°.

The powder XRD patterns for Pt/Nb_2O_5-C catalysts are shown in Figure 4.10(a). A typical broad diffraction peak for hexagonal Vulcan carbon XC-72 (Figure 4.10(c)) is not clearly observed at 24.8° due to Nb_2O_5 being superimposed on that peak. XRD coupled with the Rietveld analysis on Nb_2O_5 revealed the presence of monoclinic and orthorhombic phases shown in Figure 4.10(a). The intensity of the peak assigned to Nb_2O_5 at 2θ = 22°in Figure 4.10(a) has reduced significantly when compared with that in Figure 4.10(c), as this is due to the presence of platinum which may have overshadowed this peak.

The X-ray diffractographs of Pt/Nb_2O_5-C showed peaks at 2θ = 40.1° (111), 46.6° (200), 68.1° (220) 81.7° and (222) are indexed to the face-centered cubic structure of Pt crystallites present in Pt/Nb_2O_5-C. However, the peak of 2θ = 85° (311) is much less intense than that in Pt/C as shown in Figure 4.10(b). The XRD peaks corresponding to Pt particles are superimposed on Nb_2O_5 reflections at 2θ = 47.64°.

XRD patterns for the Pt/Ta_2O_5-C catalyst show much more intensity than the Pt peaks. The two overlapping peaks at approximately 2θ = 50° in the XRD patterns of Pt/Ta_2O_5-C confirmed the presence of the orthorhombic phase of Ta_2O_5 as seen by Huang et al. [145] in Appendix B. Figure 11 reflects the comparison of Ta_2O_5 (a), Pt/C (b) and Pt/Ta_2O_5-C(c). The peak of 2θ = 85° (311) is diminished in Figure 11.c and the Vulcan carbon XC-72 peak is non-existent in the presence of Ta_2O_5 in a Pt/Ta_2O_5-C material, this shown in Figure 11.c. The X-ray diffractographs of Pt/Ta_2O_5-C also showed peaks at 2θ = 40.1° (111), 46.6° (200), 68.1° (220) 81.7° and (222) which reflects the presence of Pt particles. The peak intensity of Ta_2O_5 has shown to be much greater than that of Nb_2O_5 and ZrO_2. In all instances when Pt is introduced the the peaks of the metal oxide support diminishes.

Zirconium dioxide exists in three polymorphic phases which are monoclinic, tetragonal and cubic. The monoclinic and tetragonal phases dominate however as shown in Figure 4.12(a). There is no shift in any of the diffraction peaks of platinum in the Pt-ZrO_2/C catalyst indicating the addition of ZrO_2 had no effect on the crystalline lattice of platinum.In the 2theta regions between 20 and 40˚ of Pt/ZrO_2-C, only ZrO_2 peaks are present. Although, at 2theta regions of 40 and 90˚ the Pt peaks are more dominant.

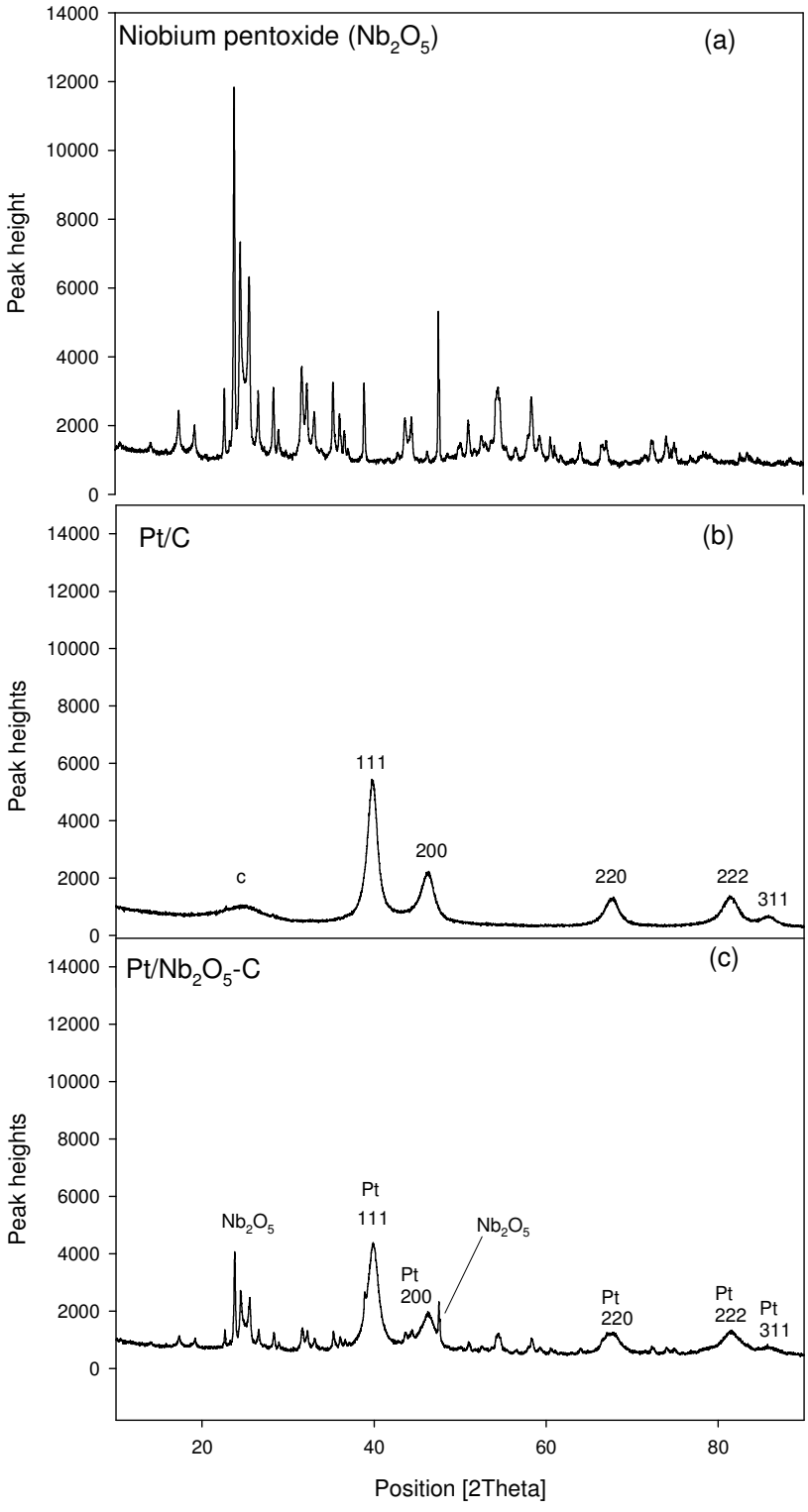

Figure 4.10 X-ray diffractographs of Nb_2O_5 (a), Pt/ C (b) and Pt/Nb_2O_5-C (c)

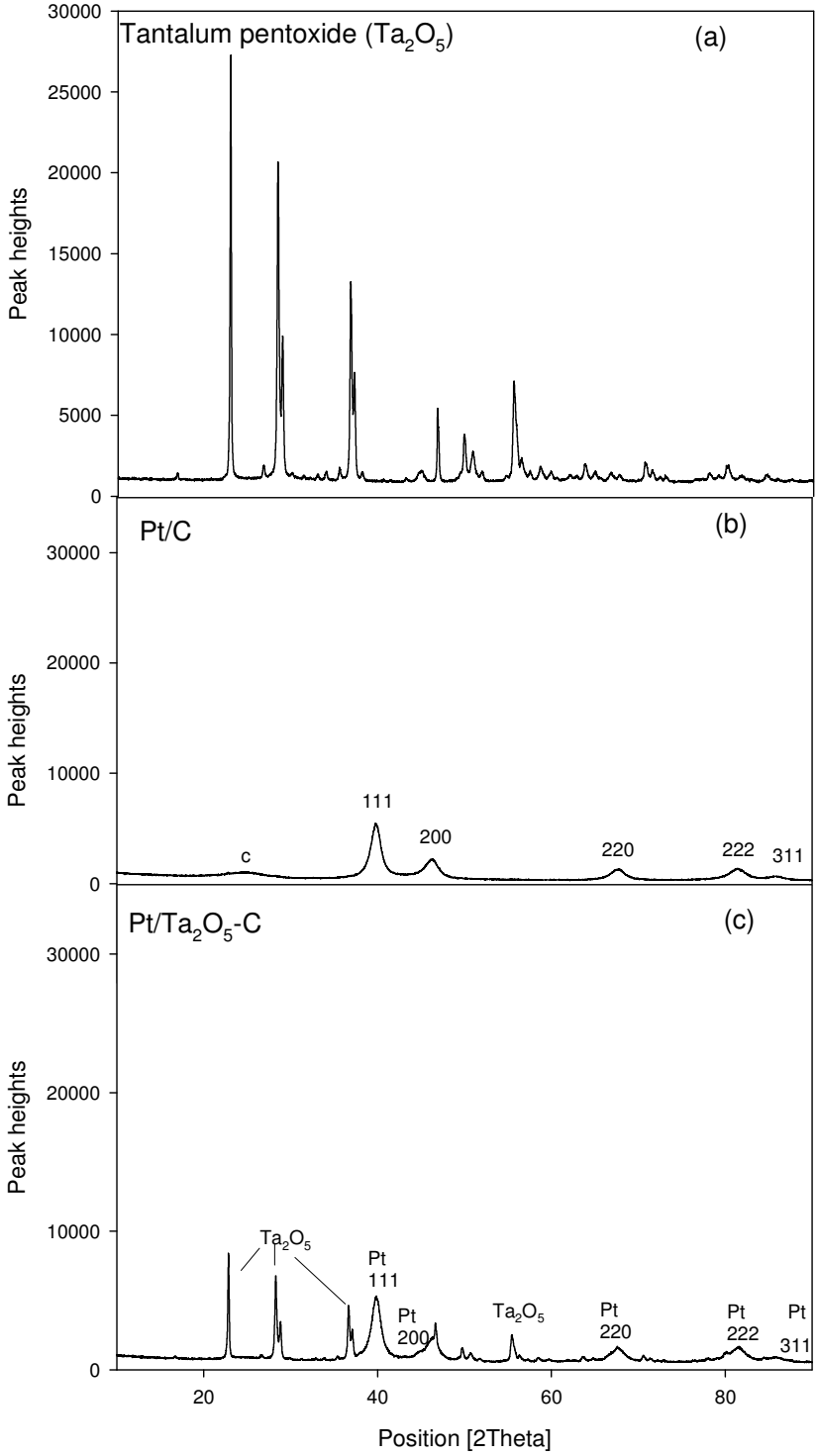

Figure 4.11 X-ray diffractographs of Ta_2O_5 (a), Pt/C (b) and Pt/Ta_2O_5-C (c)

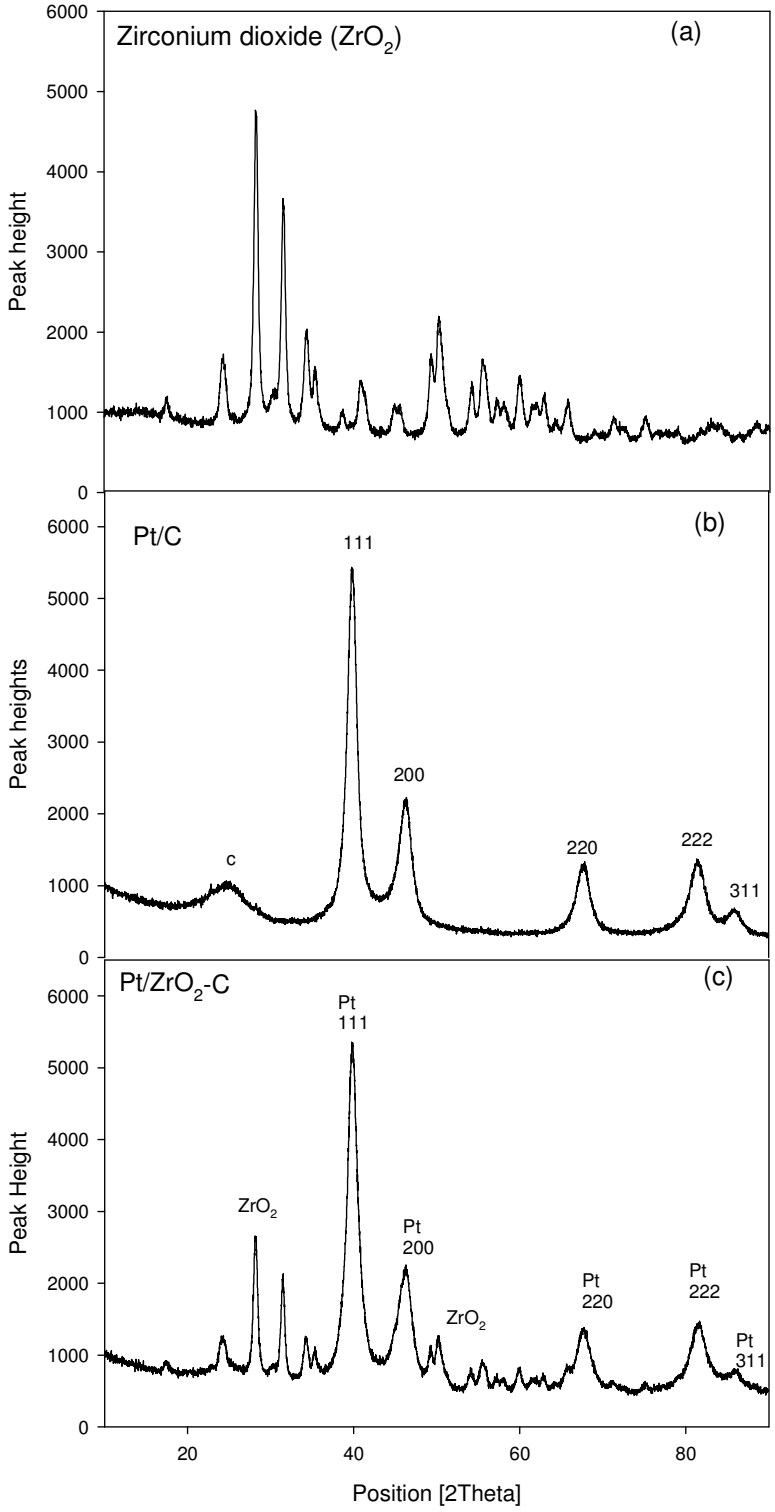

Figure 4.12 X-ray diffractographs of ZrO_2 (a), Pt/C (b) and Pt/ ZrO_2-C (c)

For the patterns of Pt/ZrO_2-C, the diffraction peaks of Pt, ZrO_2 and Vulcan carbon XC72 can be observed indicating their coexistence in the sample shown in Figure 4.12(c). The characteristic peaks of face centered cubic crystalline platinum at about 39°, 46°, 68°,81° and 85° are corresponding to the Pt(111), (200), (220),(222) and (311) planes respectively.

We then conducted a quantitative analysis of Pt, metal oxide and carbon for our four catalysts. The average crystalline size was calculated from the broadening (β) of XRD peaks using the Williamson and Hall method to separate strain (ε) and size (d) contribution to the line width.

$$\beta \cos(\beta) = \frac{\lambda}{d} + 2\varepsilon sin\theta \quad 4.1$$

When the strain is negligible (as it is for our samples), this equation can be reduced to the Scherrer formula and the surface areas of catalyst can be estimated form the X-ray diffraction peaks using the following equations:

$$d = \frac{k\lambda}{\beta_{1/2}} cos\theta \quad 4.2$$

$$S = \frac{6000}{pd} \quad 4.3$$

Where d is the average particle size (nm), S the surface area (m^2g^{-1}), λ is the wavelength of X-ray radiation (Å), p is the Pt density ($21.4g.cm^{-3}$), and θ is the angle at the position of the peak maximum, $\beta_{1/2}$ the width (in radians) of the diffraction peak at half height and k is the coefficient taken as 1. It is important to remember that the crystallite size, calculated from XRD data relates to the area of coherent diffraction and can in general be smaller than the true particle size [146].

Table 4.3 The true metal ratio and crystal sizes of the catalyst

	Metal ratio	Crystal size(nm)
Pt:C	50:50	6.39
Pt:Nb_2O_5:C	35:38.1:26.9	5.50
Pt:Ta_2O_5:C	35:28.3:36.7	7.21
Pt:ZrO_2:C	35:31.4:33.6	6.06

The experimental metal ratios and the metal ratios given by XRD were quite similar. The experimental metal ratios are given in Table 3.1 and the actual metal ratios are provided in Table 4.1.

4.2 Cyclic voltammetry

4.2.1 Electrochemical Active Surface Area (EAS)

CV scans are presented as a voltammograms of current (A) vs. applied potential (V). The voltammogram exhibits multiple peaks associated with both the oxidation and reduction reactions. Each peak is indicative of the adsorption onto or desorption from a particular crystal index of platinum. From the CV scans, we were able to determine the EAS for the different catalysts. EAS was determined with the EC-Lab (V9.55) integral tool by selecting two points on the CV over which the integral had to be determined.

EAS of the catalyst could be estimated from the coulombic charge for the hydrogen adsorption and desorption (Q_H) in the cyclic voltammograms. Q_H is the charge for the hydrogen desorption ($mC.cm^{-2}$).The value of (Q_H) is calculated as the mean value between the amounts of charge transfer during the electro-adsorption and desorption of H_2 Pt sites.

$$EAS = \frac{Q_H}{[Pt]\times 0.210} \qquad 4.4$$

Where [Pt] represents the platinum loading ($mg.cm^{-2}$) on the electrode, and 0.21 represents the charge required to oxidise a monolayer of H_2 on smooth Pt [138]. The units used for the EAS were cm^2/mg.

Pt area loss is defined as

$$R_{A,loss} = 1 - \frac{A_{Pt,post}}{A_{Pt,prior}} \qquad 4.5$$

A reduction in the peak area indicates a reduction of peak active sites due to agglomeration of metal particles on the support, dissolution of metal in the electrolyte or deactivation of active sites through coverage with SO_2, which tends to poison the catalyst thereby inhibiting bulk SO_2 oxidation [19]. The cyclic voltammograms of Pt/C (a), Pt/Nb_2O_5-C (b), Pt/Ta_2O_5-C (c) and Pt/ZrO_2-C (d) used to calculate the electrochemical active surface area are shown in Figures 4.13.

Table 4.2 The Pt loading, electrochemical active surface area and Pt area loss

Catalysts	Pt loading ($mg.cm^{-2}$)	Prior EAS (cm^2/mg)	Post EAS (cm^2/mg)	Pt loss	Retention of EAS %
Pt/C	0.06103	367.95	332.19	0.0972	90.28
Pt/Nb_2O_5-C	0.06192	354.74	338.76	0.0451	95.28
Pt/Ta_2O_5-C	0.06178	210.49	204.39	0.0289	97.10
Pt/ZrO_2-C	0.06133	392.09	275.78	0.2966	70.34

The EAS of Pt/ZrO_2-C was greater than that of Pt/Nb_2O_5-C, Pt/Ta_2O_5-C, and Pt/C which can be explained by the smaller crystal sizes of Pt/ZrO_2-C. However, Pt/ZrO_2-C experienced the highest area loss which explains the inferior catalytic activity as shown in paragraph 4.7.2, because Pt/ZrO_2-C was able to retain only 70.34% of its EAS area.

The observed trend for EAS depends on our calculation and the amount of platinum loaded on the electrode. However, Pozio *et al*. [146] stated that as platinum loading increase, electrode thickness grew and as a consequence some platinum particles were blocked in the carbon substrate and not exposed to the electrolyte solution. On the other hand if a small amount of catalyst powder did not cover the electrode geometric area uniformly, then the EAS was large.

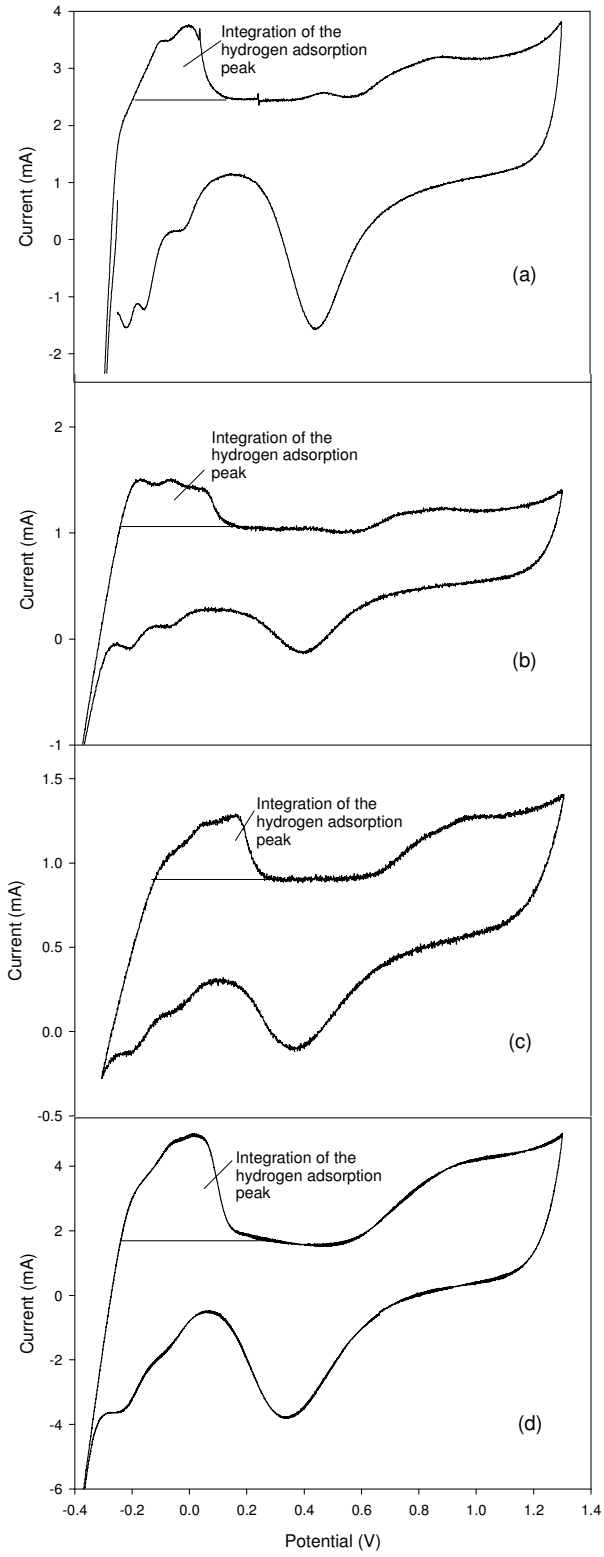

Figure 4.13 CV scans of Pt/C (a), Pt/Nb_2O_5-C (b), Pt/Ta_2O_5-C (c) and Pt/ZrO_2-C (d) in 0.1M$HClO_4$ at 25°C

4.2.2 Pt dissolution

ICP-OES (iCAP 6000 series Thermo scientific Duo utilising iTEVA) was used to determine the amount of Pt, from the four catalysts, dissolved in the various electrolytes at different temperatures. Table 4.3 shows the average Pt concentration. Each electrochemical run was conducted in 100ml of 1.0M H_2SO_4 electrolyte at 30˚C with potential ranging between -0.3 to 1.8V and a scan rate of 20mV/s.

Table 4.3 Pt dissolution concentration in the 1.0M H_2SO_4 electrolyte at 30˚C

Catalysts	Pt Concentration (ppm)
Pt/C	0.0639
Pt/Nb_2O_5-C	0.1825
Pt/Ta_2O_5-C	0.1274
Pt/ZrO_2-C	0.2800

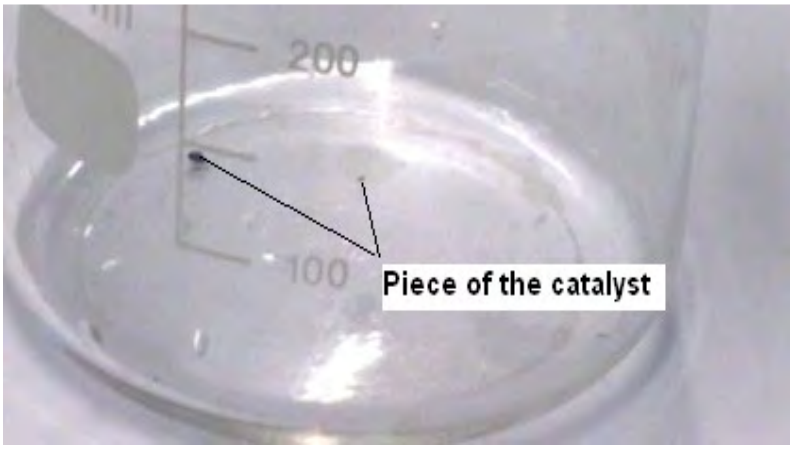

Figure 4.14 Catalyst mechanical fault

Figure 4.14 shows the catalyst material that had fallen off from the glassy carbon insert as part of the working electrode. This mechanical fault was observed for the Pt/ZrO_2-C catalyst after the final LP scan. This reveals that the preparation of the catalyst was not fully effective.

4.3 Stability tests

Stability tests were not conducted for this study. However, the studies conducted to determine the electrochemical active surface area and Pt dissolution are clear indications that there was same degree of instability with regard to the catalysts during the execution of the experiments.

4.4 Catalyst testing

The original linear polarisation scans were plotted as applied potential (V) versus current (A). The current density is the quotient of current and the smooth surface area of the catalyst (0.1964cm^2). Although the reference electrode was Ag/AgCl, the working electrode potential was corrected to that of the standard hydrogen electrode (SHE) to ease the interpretation of the electrochemical results. The current density values that are used for plotting the influence of sulphuric acid concentration and temperature graphs (shown in Section 4.6.1) are taken from the linear polarisation scans at 1.0 and 1.8V as shown in Figures 4.15 to 4.18 and in Appendix D.

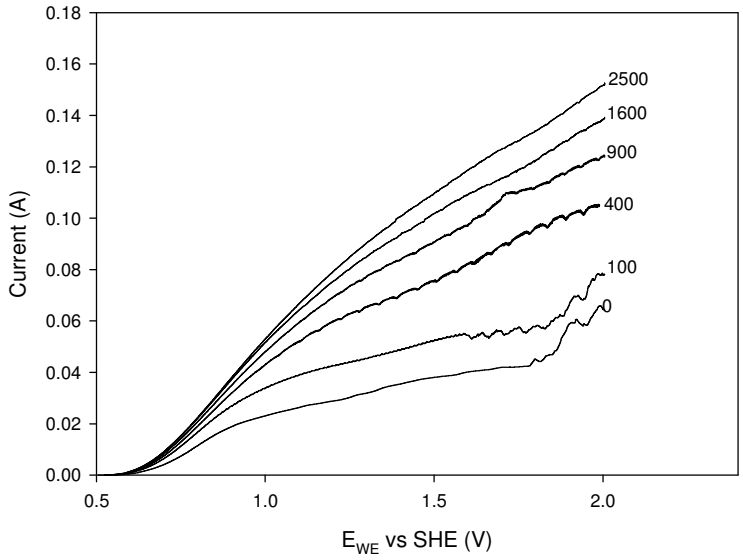

Figure 4.15 LP scan of Pt/ZrO_2-C at different rotation speeds and SO_2 was bubbled in 1.5M H_2SO_4 at 30°C

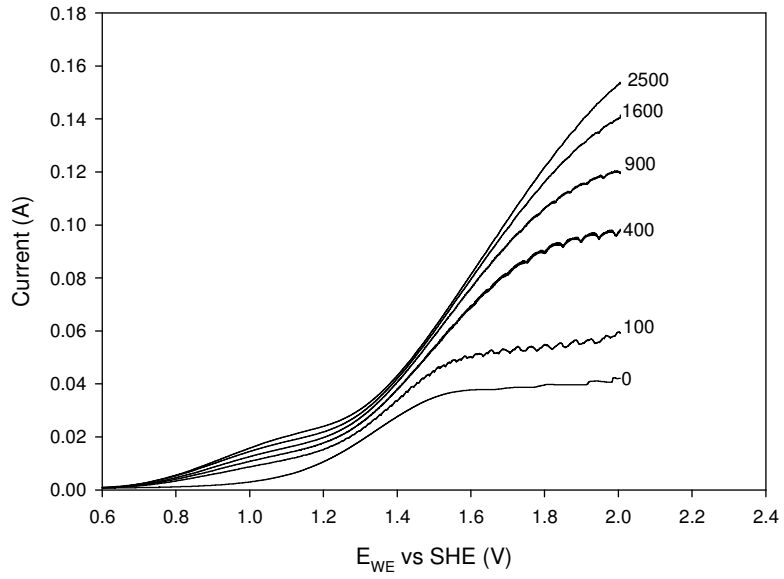

Figure 4.16 LP scan of Pt/C at different rotation speeds and SO_2 was bubbled in 1.5M H_2SO_4 at 30°C

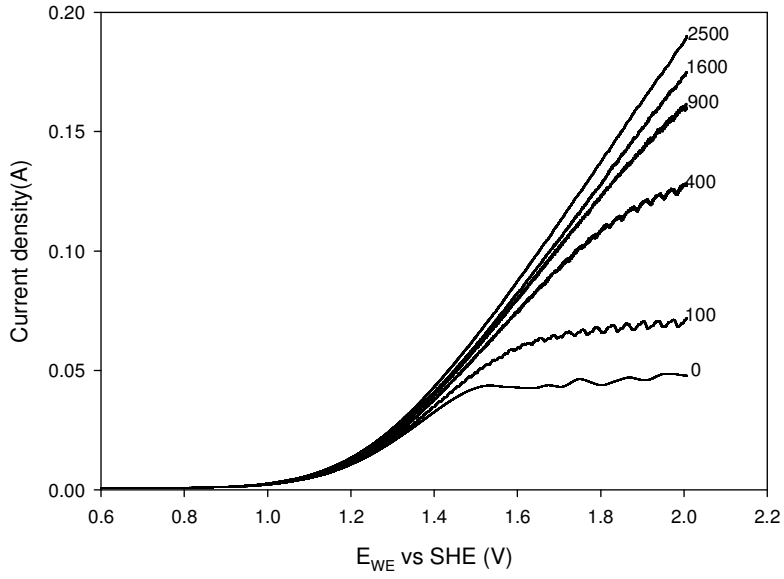

Figure 4.17 LP scan of Pt/Ta_2O_5-C at different rotation speeds and SO_2 was bubbled in 1.5M H_2SO_4 at 30°C

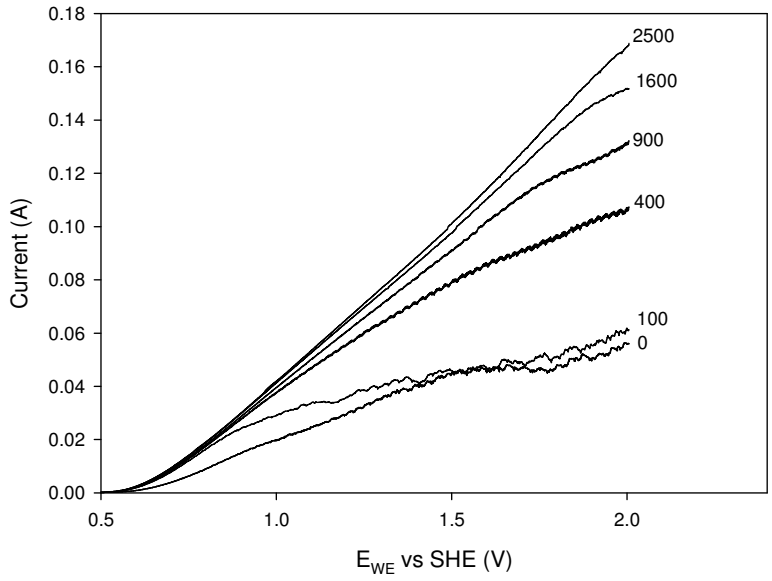

Figure 4.18 LP scan of Pt/Nb_2O_5-C at different rotation speeds and SO_2 was bubbled in 1.5M H_2SO_4 at 30°C

4.4.1 Influence of sulphuric acid concentration and temperature

At 0rpm Figure 4.19 reveals that there was an increase of current density with an increase of H_2SO_4 concentration and temperature. Current densities at 1.0 and 1.8V at both 20˚C and 30˚C increased and as compared to the increase from 0.5M to 1.0M, the current density increase was much higher from 1.0M to 1.5M.

However, the increase of current densities as a result of temperature increments showed a slight consistency even though the increase was not enormous as expected. There was an unexplainable “glitch” that had occurred for Pt/C at 1.0V in 0.5M H_2SO_4 at 20˚C at most rotation speeds.

At 1.0V Figure 4.20 shows that there was a direct dependence of current density on concentration at 900rpm. However in 1.0M H_2SO_4 at 1.8V at 20˚C and 30˚C, there was a deviation from the current density and sulphuric acid relation even though current density increased with increased concentration.

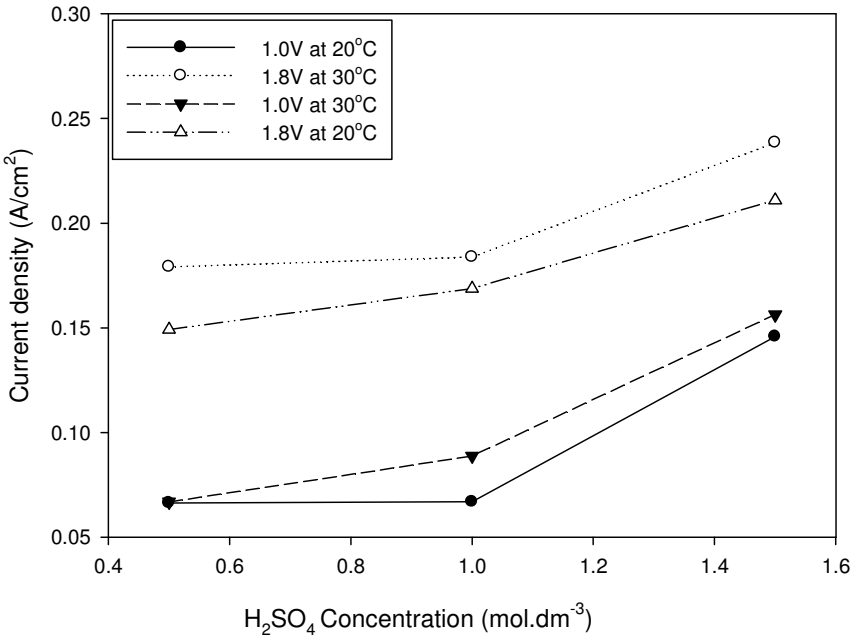

Figure 4.19 Influence of acid concentration and temperature of Pt/C at 0rpm

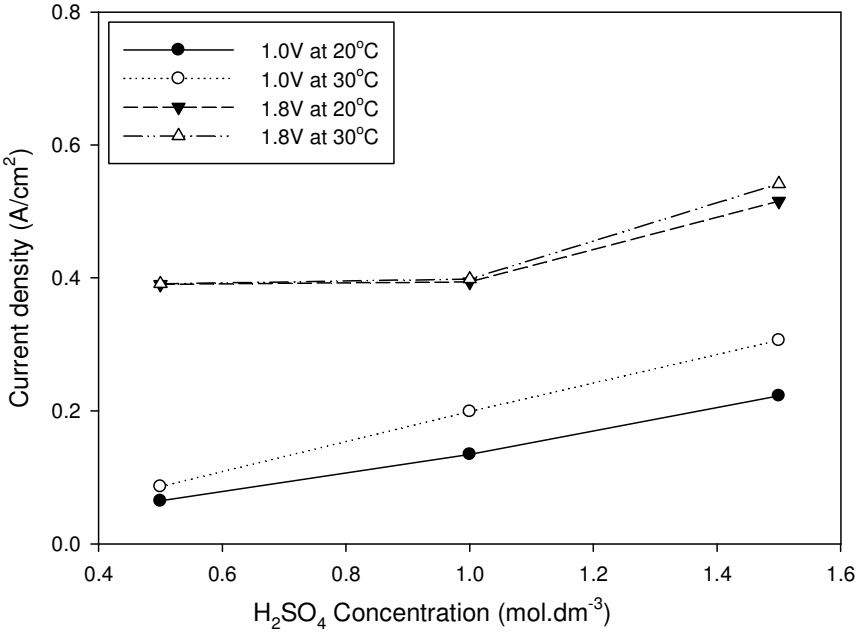

Figure 4.20 Influence of acid concentration and temperature of Pt/C at 900rpm

At rotation speeds of 1600 and 2500rpm, Figures 4.21 and 4.22 showed that the current density increase between 20˚C and 30˚C at 1.0V in 0.5M H_2SO_4 was minimal compared to the vast current density gap between 1.0M and 1.5M.

In Figure 4.24, a comparison of 1.0V and 1.8V were plotted and Figure 4.25 illustrates the current densities gaps of 1.6 and 1.8V. Different potentials, 1.0 and 1.6V, were intentionally selected to verify the increase of current density due to the influence of sulphuric acid and temperature irrespective of potential selected (1.0 or 1.6V).

The temperature influence on the catalytic performance on Pt/Nb_2O_5-C showed an increase in current density from 20˚C to 30˚C at all tested sulphuric acid solutions as revealed in Figure 4.23 to 4.25. However, between the rotation speeds of 100 (shown in Appendix C) and 400rpm, there was a minimal increase in current density from 0.5M to 1.0M H_2SO_4 as compared to the significant increase at other rotation speeds.

At 1.0V, the current density gap between 20 and 30˚C showed an improvement with the increase of the sulphuric acid concentration. This was applicable at 0 and 400 rpm shown in Figures 4.23 and 4.24. Although at 1.0V the catalytic activity enhancement for Pt/Nb_2O_5-C at 0rpm was visible, there appeared to be a wider increase at 0.5M than at 1.5M from 20 to 30˚C shown in Figure 4.23. This reflects how the influence of temperature on the catalytic activity of Pt/Nb_2O_5-C was not as consistent as that for the sulphuric acid concentration.

The graph in Figure 4.24 shows the influence of acid concentration and temperature on the catalytic activity of Pt/Nb_2O_5-C at 400 rpm. Pt/Nb_2O_5-C showed an increased current density at 20˚C from 425.67 to 520.76 and 544.23mA.cm^{-2} from 0.5M to 1.0M and 1.5M respectively as. The current density gap increase from 1.0M to 1.5M resembles that from 0.5 to 1.0M H_2SO_4 for both temperatures in magnitude.

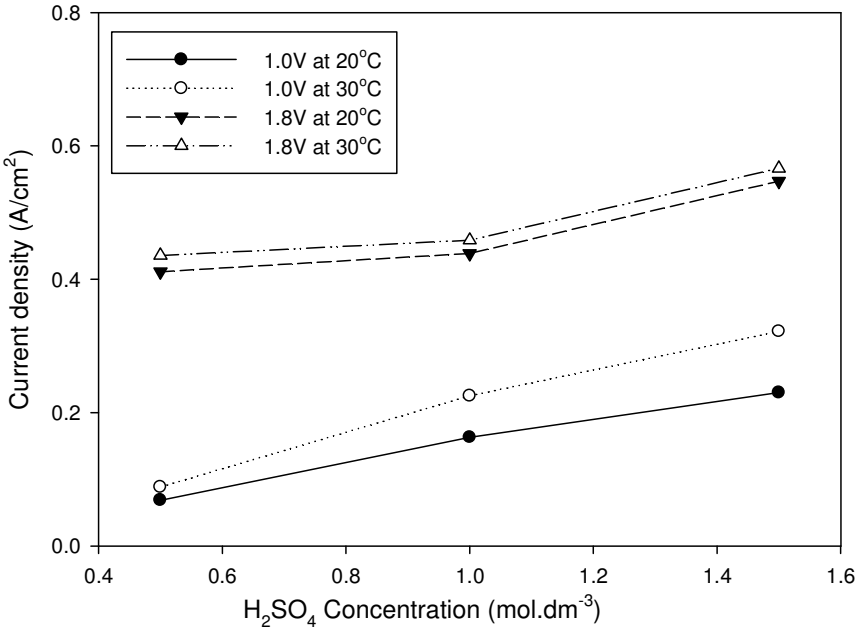

Figure 4.21 Influence of acid concentration and temperature of Pt/C at 1600rpm

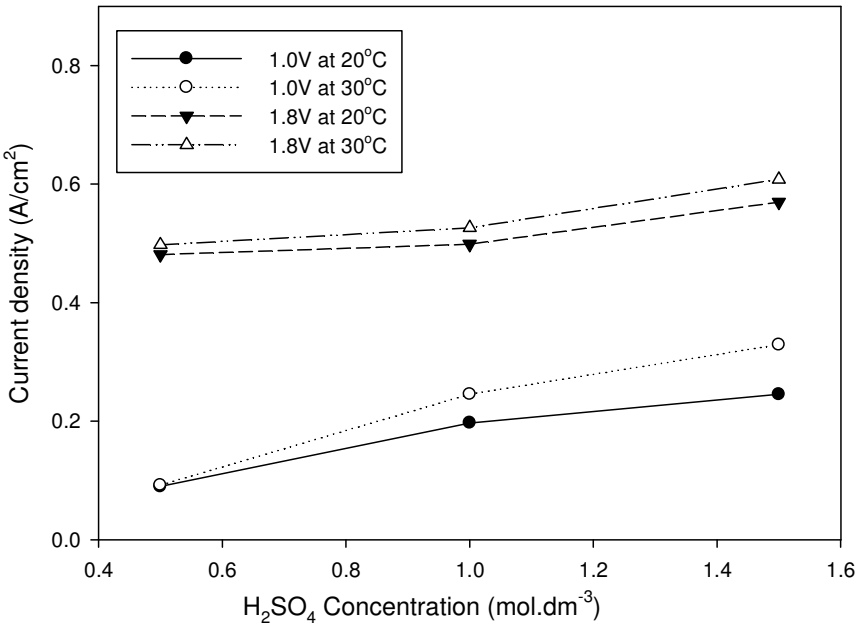

Figure 4.22 Influence of acid concentration and temperature of Pt/C at 2500rpm

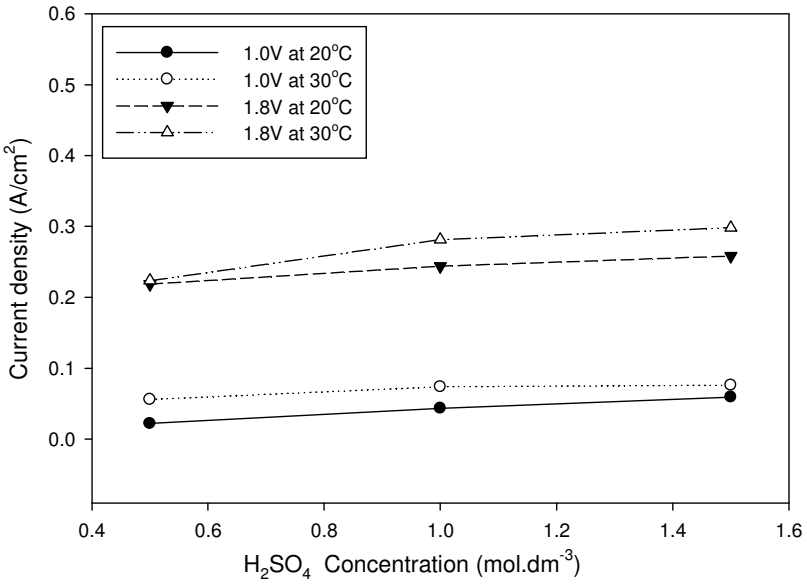

Figure 4.23 Influence of acid concentration and temperature of Pt/Nb_2O_5-C at 0rpm

Figure 4.27 shows the expected increase as a result of the increase in sulphuric acid concentrations and a slight improvement of current density in all the tested sulphuric acid solutions due to the increase in temperature.

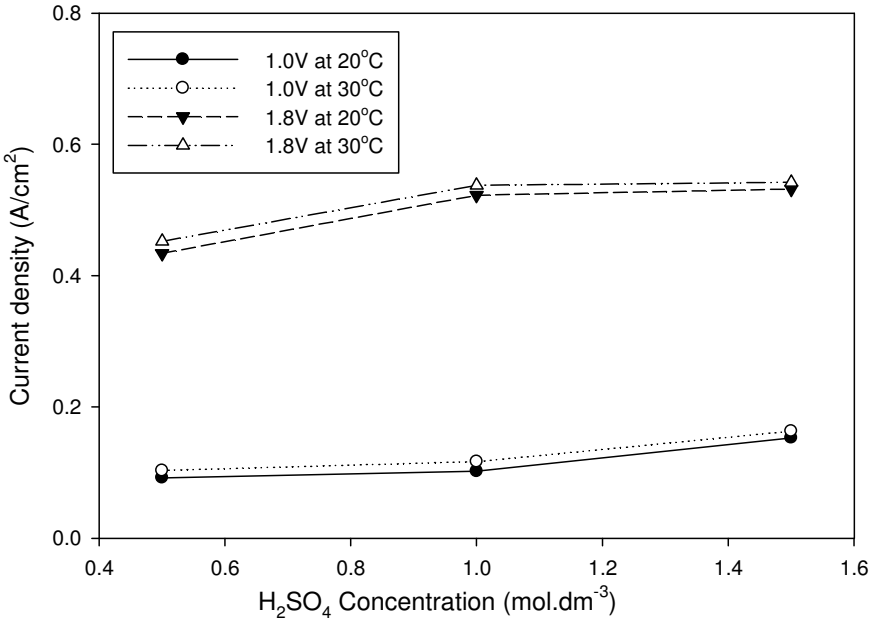

Figure 4.24 Influence of acid concentration and temperature of Pt/Nb_2O_5-C at 400rpm

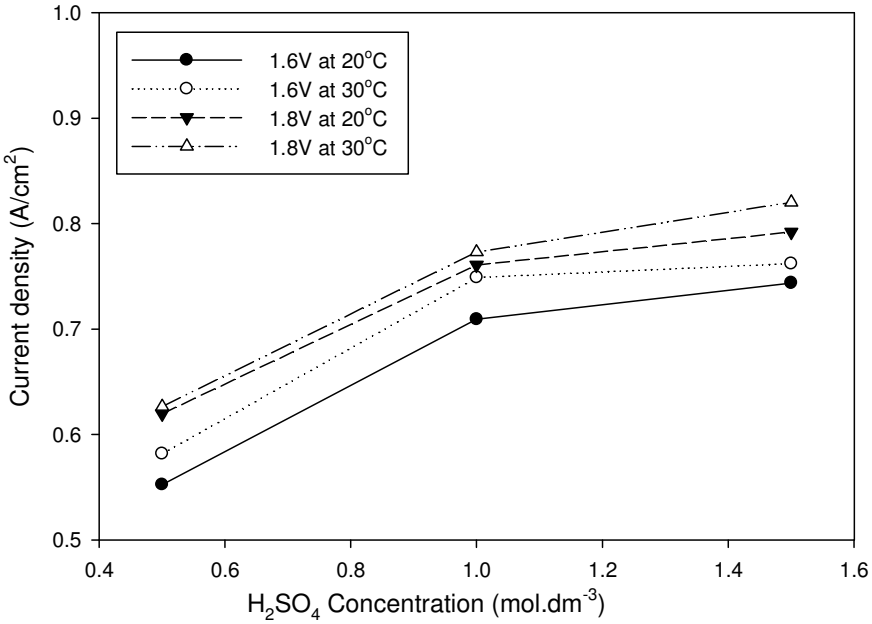

Figure 4.25 Influence of acid concentration and temperature of Pt/Nb_2O_5-C at 2500rpm

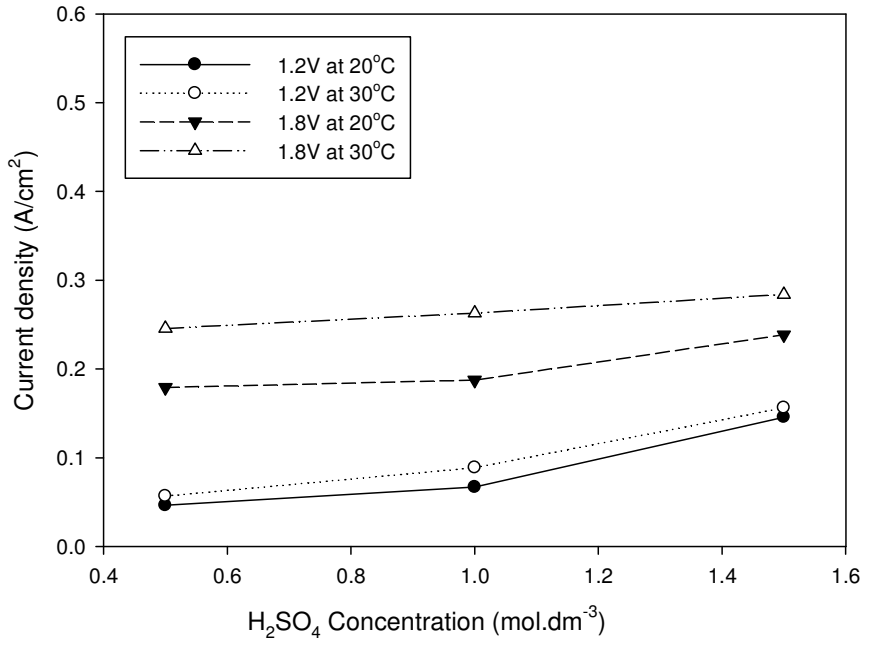

Figure 4.26 Influence of acid concentration and temperature of Pt/Ta_2O_5-C at 0rpm

Pt/Nb_2O_5-C experienced an even increase from 0.5M to 1.0 to 1.5M H_2SO_4 at 20˚C and 30˚C, although the increase at 1.0M from 20˚C to 30˚C was observed to be somewhat

out of range when compared to the rest of the points in this graph. At potential of 1.6V, Figure 4.25 shows a minimal rise from 1.0M to 1.5M H_2SO_4 at 30˚C.

In summary, results showed that Pt/Ta_2O_5-C showed better performance with the increase of acid concentration and temperature at all rotation speeds. The collection of graphs (in Appendix C) reflecting the impact of acid concentration and temperature for the Pt/Ta_2O_5-C at rotation speeds 100, 900, 1600 and 2500rpm also share the same conclusion as the ones displayed here.

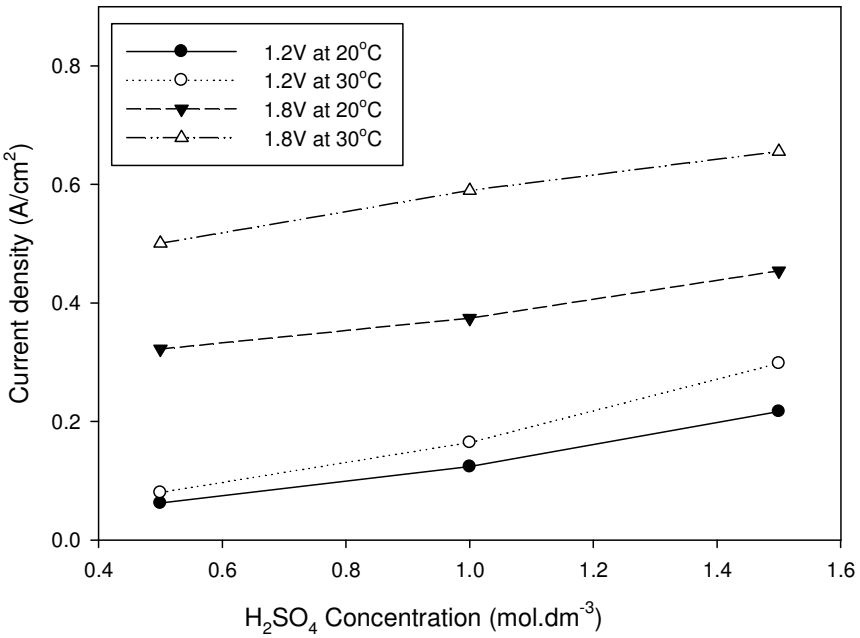

Figure 4.27 Influence of acid concentration and temperature of Pt/Ta_2O_5-C at 400rpm

There is a clear indication that the increase in acid concentration and temperature had a positive influence (at 900rpm) on the catalytic performance of Pt/ZrO_2-C at 20˚C. The current densities of 363.45, 407.49 and 456.03 $mA.cm^{-2}$ increased substantially to 398.7, 506.07 and 673.35 $mA.cm^{-2}$ from 0.5M to 1.0M and from 1.0M to 1.5M H_2SO_4 at 30˚C (as shown in Appendix C).

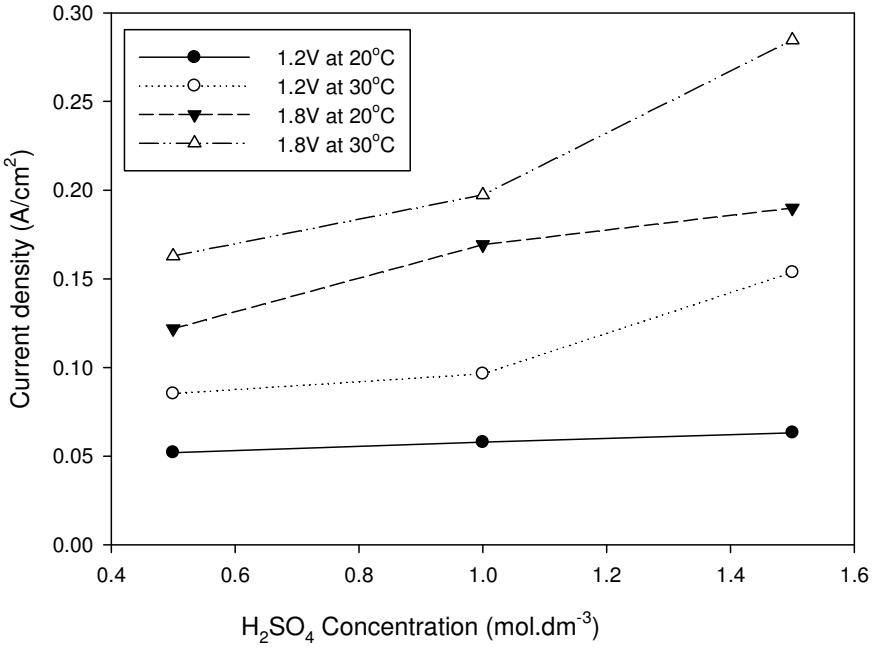

Figure 4.28 Influence of acid concentration and temperature of Pt/ZrO_2-C at 0rpm

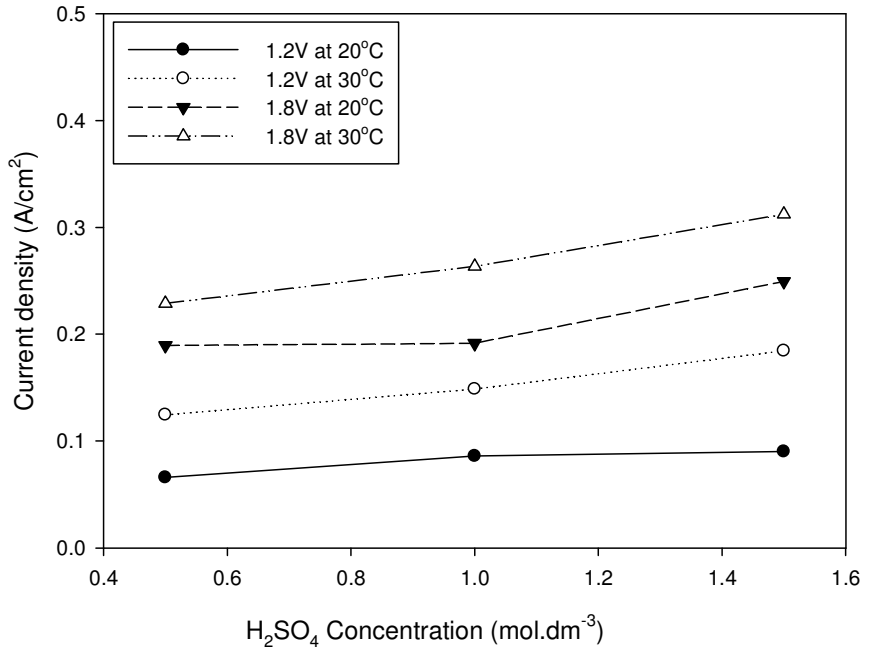

Figure 4.29 Influence of acid concentration and temperature of Pt/ZrO_2-C at 100rpm

Figures 4.28 and 4.29 depict the influence on the catalytic activity of Pt/ZrO_2-C as a result of the gradual increase of sulphuric acid from 0.5M to 1.5M at 20 and 30˚C. The

graphs also reflect that with the gradual increase of applied potential, the current density was slightly increased for both the displayed graphs and those placed in Appendix

In conclusion, the influence of acid concentrations of 0.5M to 1.5M H_2SO_4 and temperature of 20˚C and 30˚C on Pt/C, Pt/Nb_2O_5-C, Pt/Ta_2O_5-C and Pt/ZrO_2-C was positive. Appendix C also shows how temperature and sulphuric acid concentration positively influenced the electrochemical performance of Pt/C, Pt/Nb_2O_5-C, Pt/Ta_2O_5-C and Pt/ZrO_2-C.

Considering Figures 4.27 and 4.28 it is clear that though Pt/ZrO_2-C exhibited the least improvement as a result of the increase in temperature and sulphuric acid concentration, Pt/ZrO_2-C exhibited a huge difference between 20˚C and 30˚C at 1.2 and 1.8V.

4.4.2 Levich experiments

The Levich equation predicts that the limiting current is proportional to the square root of rotation rate.

$$\mathrm{I}_{\mathrm{lim,c}} = 0.620nFAD^{2/3}v^{-1/6}\omega^{1/2}C_o^b \qquad 2.17$$

Where $\mathrm{I}_{\mathrm{lim,c}}$is the limiting current (A), n the number of electrons exchanged in the reaction, F the Faraday constant (96485C.mol^{-1}), A the electrode surface area (m^2), D the diffusion coefficient (m^2/s). If known the diffusion coefficient can be used in the Levich equation to find the number of electrons involved in the overall oxidation reaction, which can be indicative of the expected reaction product. ω is the rotation rate of the electrode (rad.s^{-1}), v represents the kinematic viscosity of the electrolyte and C_o^b the concentration of the reacting SO_2 (mol.m^{-3}) in the sulphuric acid solution. The Levich equation is used for fast electron transfer.

The experimental results showed considerable disobedience to the Levich equation. The Levich plots revealed that at potentials V = 1.74, 1.75, 1.76, 1.79 and 1.80, there is a visible deviation from the Levich equation, whereas at potential V = 1.0 there is some correlation to the Levich equation.

Levich graphs of all the prepared catalysts in 0.5M H_2SO_4 at 20℃ are given below in Figures 4.30 to 4.33 and the results deduced from the graphs such as the number of

electrons transferred and the heterogeneous rate constant are given in table 4.4 to 4.7. The rest of the graphs and tables are given in Appendix D and E, respectively.

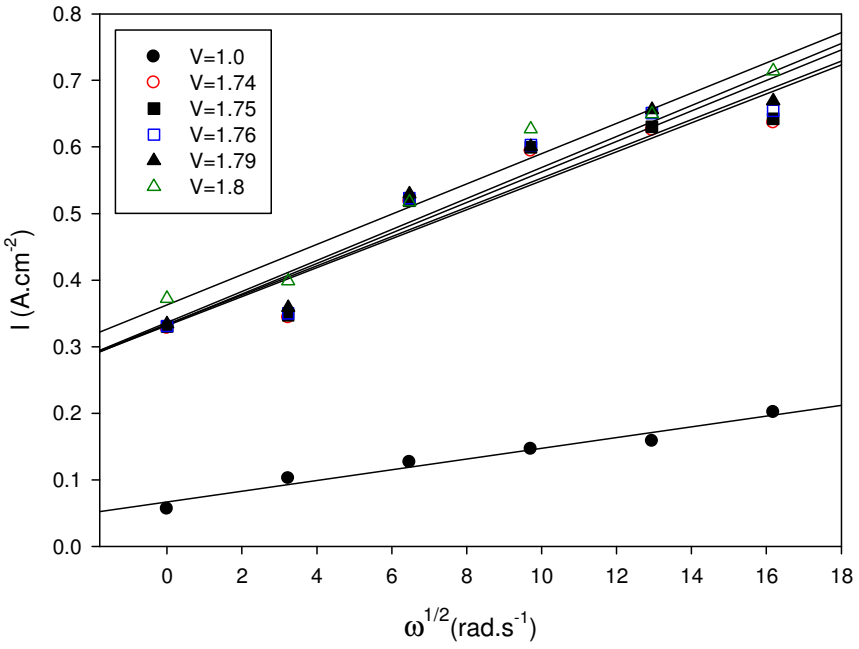

Figure 4.30 Levich plots of Pt/C in 0.5M H_2SO_4 at 20˚C

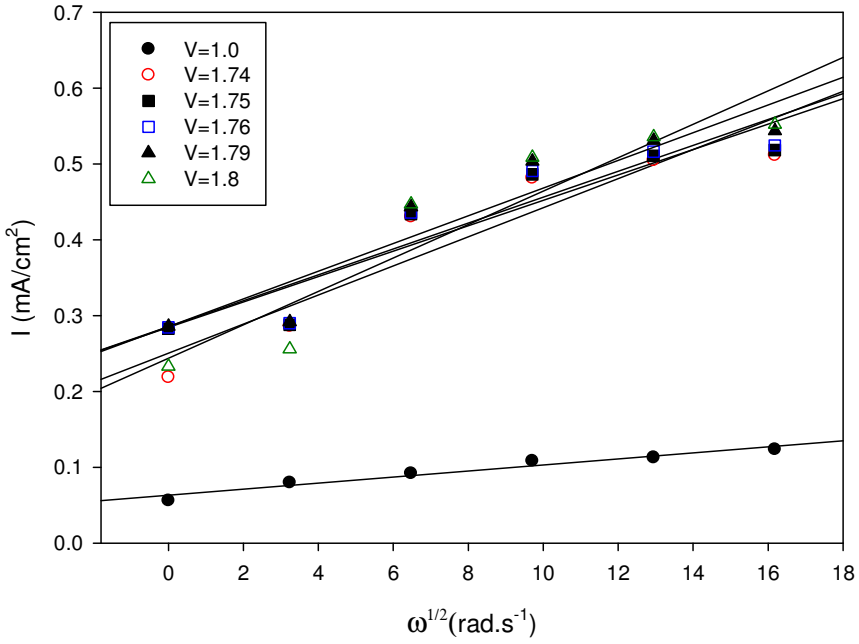

Figure 4.31 Levich plots of Pt/Nb_2O_5-C in 0.5M H_2SO_4 at 20˚C

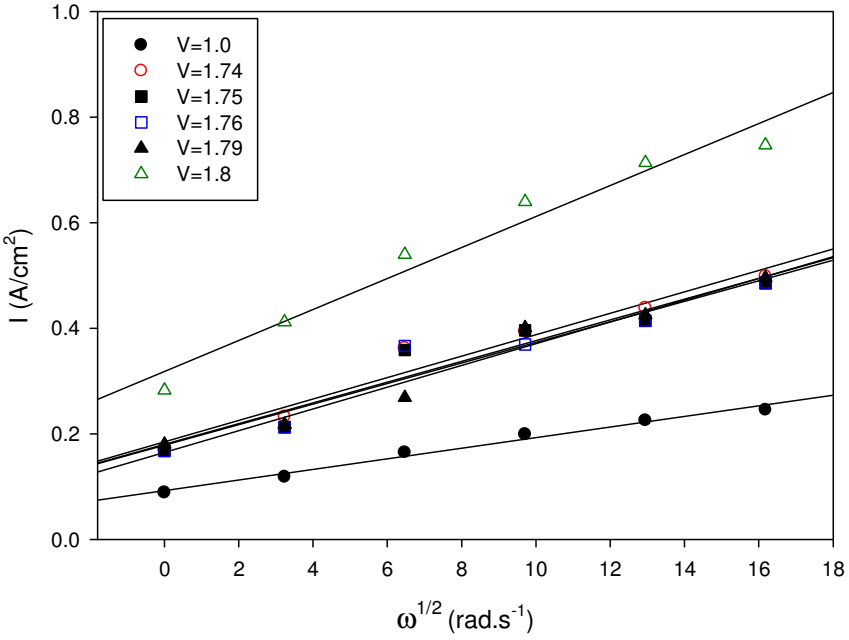

Figure 4.32 Levich plots of Pt/Ta_2O_5-C in 0.5M H_2SO_4 at 20˚C

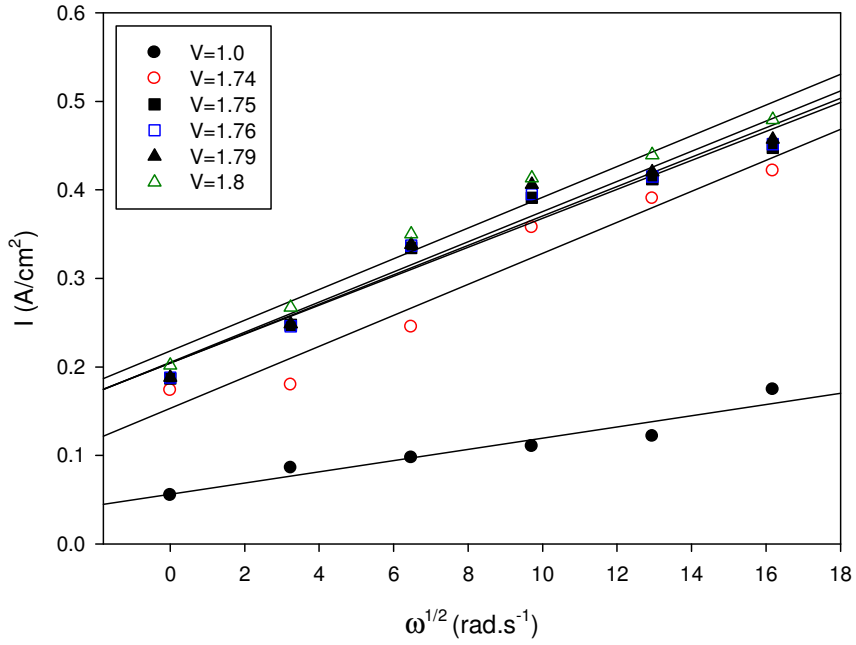

Figure 4.33 Levich plots of Pt/ZrO_2-C in 0.5M H_2SO_4 at 20˚C

The relation between the peak height and square root of the scan rate is roughly linear at all potentials selected for plotting this graphs, except at 1.0V. This is true for all the Levich plots suggesting that at 1.0 the reaction rate is not only limited by the mass transfer to the electrode.

4.4.3 Koutecky-Levich experiments

The Koutecky-Levich equation (Equation 2.18) is applicable to surface reactions obeying strictly to the first order reactions kinetics, the reactions therefore are too slow to allow for convective-diffusion control to be operative.

$$\frac{1}{\mathrm{I_c}} = \frac{1}{0.620nFAD^{2/3}\nu^{-1/6}\omega^{1/2}C_o^b} + \frac{1}{nFAk_hC_o^b} \qquad 2.18$$

I_c is the overall current density on the disk electrode, the first term of equation 3.18 is the boundary layer diffusion-limited current density and the second term represents the kinetic current density.

Koutecky-Levich graphs of the all the prepared catalysts in 0.5M H_2SO_4 at 20℃ are given below in figures 4.34 to 4.37. The rest of the graphs for all the sulphuric acid concentrations at different temperatures are given in Appendix D. The Koutecky-Levich plots are given as the relation between the inverse of the current density and the inverse of the rotation speeds in radians per second. From the Koutecky-levich plots we observed that only at the potential of 1.0V, there was a deviation. This means that the inverse of current density roughly increased with the inverse of the rotation rate. This had to do with the kinetic dimensions at this region. From the regression line information of these graphs together with the Levich plots, the slope and y intercepts are used to calculate the number of electrons transferred during the reaction and the heterogeneous rate constant. This information is provided below in Tables 4.4 to 4.7. The calculation example is provided in Appendix E.

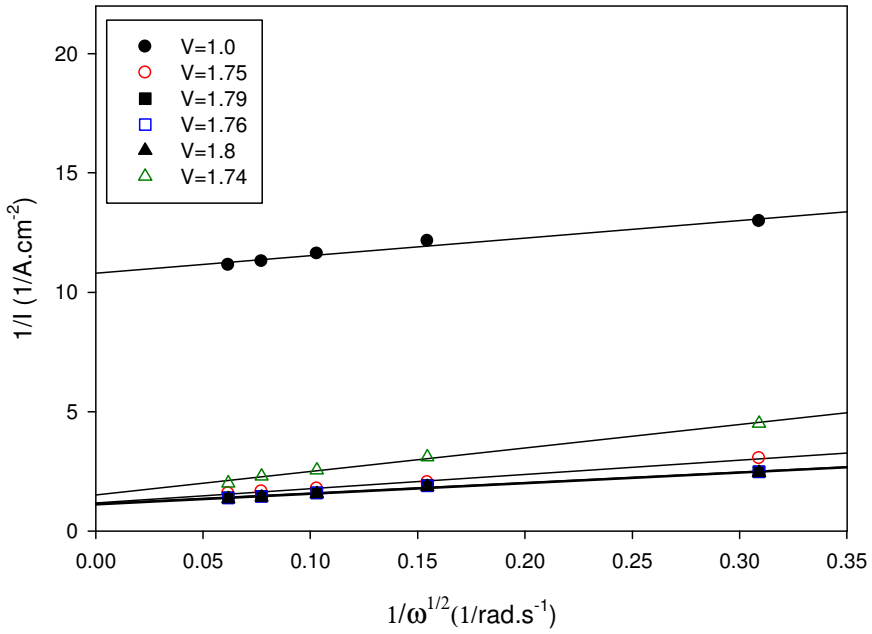

Figure 4.34 Koutecky-Levich plots of Pt/C in 0.5M H_2SO_4 at 20˚C

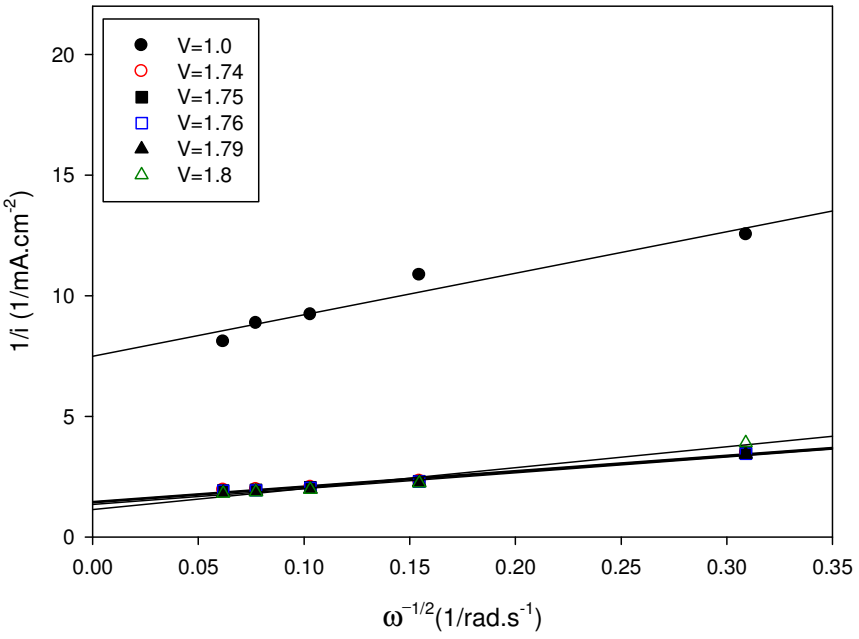

Figure 4.35 Koutecky-Levich plots of Pt/ Nb_2O_5-C in 0.5M H_2SO_4 at 20˚C

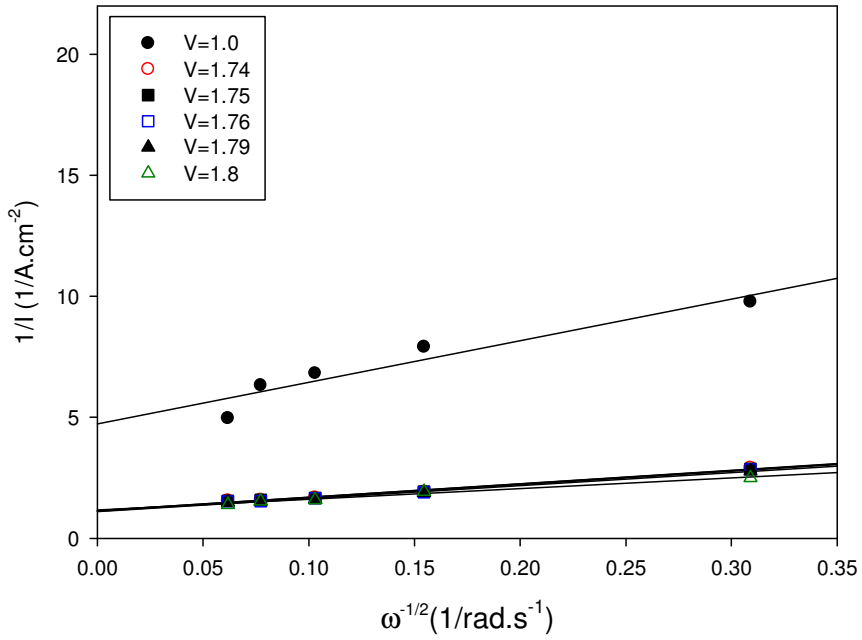

Figure 4.36 Koutecky-Levich plots of Pt/Ta_2O_5-C in 0.5M H_2SO_4 at 20˚C

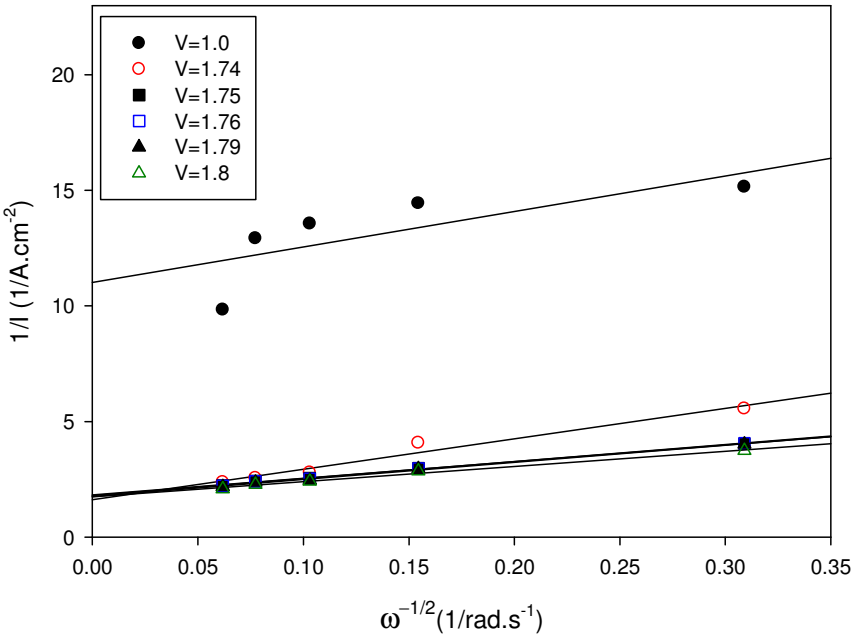

Figure 4.37 Koutecky-Levich plots of Pt/ZrO_2-C in 0.5M H_2SO_4 at 20˚C

Table 4.4 The number of electrons transferred and heterogeneous rate constant of Pt/C at 20˚C

H_2SO_4 concentration ($mol.dm^{-3}$)	Potential (V)	Number of electrons	k_h
0.5	1.74	0.00430271	0.048096709
0.5	1.75	0.00432718	0.046859906
0.5	1.77	0.0043386	0.046335945
0.5	1.78	0.00432392	0.044952098
0.5	1.8	0.0044055	0.043165713

Table 4.5 The number of electrons transferred and heterogeneous rate constant of Pt/Nb_2O_5-C at 20˚C

H_2SO_4 Concentration ($mol.dm^{-3}$)	Potential (V)	Number of electrons	k_h
0.5	1.74	0.00456867	0.052742842
0.5	1.75	0.00465025	0.046989809
0.5	1.77	0.00468288	0.048468638
0.5	1.78	0.00465025	0.050435728
0.5	1.8	0.00473183	0.044520491

Table 4.6 The number of electrons transferred and heterogeneous rate constant of Pt/Ta_2O_5-C at 20˚C

H_2SO_4 Concentration ($mol.dm^{-3}$)	Potential (V)	Number of electrons	k_h
0.5	1.74	0.004895	0.047913941
0.5	1.75	0.00522133	0.045526338
0.5	1.77	0.00522133	0.045836041
0.5	1.78	0.00522133	0.045836041
0.5	1.8	0.0053845	0.046669423

From the data collected we conclude that the SO_2 oxidation reaction on the Pt/C, Pt/Nb_2O_5-C, Pt/Ta_2O_5-C and Pt/ZrO_2-C is a multistep reaction since the calculation for the number of electrons revealed no integers. However the value from the calculation of the heterogeneous rate constant was less than one, suggesting that this reaction is a

simple charge transfer reaction. This resulted when the species adsorbed on the electrode became saturated by adsorbed SO_2 species.

Table 4.7 The number of electrons transferred and heterogeneous rate constant of Pt/ZrO_2-C at 20˚C

H_2SO_4 Concentration ($mol.dm^{-3}$)	Potential (V)	Number of electrons	k_h
0.5	1.75	0.0017139	0.10314938
0.5	1.78	0.00163819	0.113028275
0.5	1.77	0.00180136	0.104996232
0.5	1.78	0.00180136	0.109775387
0.5	1.8	0.00196453	0.10065783

The calculations and tables showing the number of electrons transferred and heterogeneous rate constant for the rest of the experimental conditions are given in Appendix D.

4.4.4 Influence of the metal oxides on Pt/C

The influence of the different metal oxides was not only revealed during the physical characterisation such as the transmission electron microscopy but also in the electrochemical studies. The Pt/Ta_2O_5-C catalysts showed better electrochemical performance at all the tested conditions. This may be as a result of the Pt/Ta_2O_5-C having the highest Pt loading with an unexplainable lower electrochemical active surface area when compared to the other prepared catalysts. However, Pt/Ta_2O_5-C experienced the lowest Pt area loss and Pt dissolution. Tantalum pentoxide had difficulties in obtaining a uniform dispersion of Pt particles as shown by previous TEM images. In contrast, Pt/ZrO_2-C was the worst in terms of electrochemical measurements. The unexpected low catalytic activity of Pt/ZrO_2-C may be as result of the highest Pt concentration dissolved in the electrolyte and the significant Pt area loss even though prior to the linear polarisation scans, Pt/ZrO_2-C had a much higher electrochemical active surface area because of its small crystal size. Pt/C and Pt/Nb_2O_5-C had intermediate performances throughout the study. The minimal performance experienced from the Pt/C is as a result of the original form of the electrocatalyst that had large Pt crystals which may have reduced the active sites or the electrochemical active surface area.